Serre equations in channels and rivers of arbitrary cross section

Damien Violeau

Serre equations in channels and rivers of arbitrary cross section

Damien Violeau[1]

[1]EDF, 6 quai Watier, 78400 Chatou, France, Email: damien.violeau@edf.fr

[2]Laboratoire d'Hydraulique Saint-Venant, 6 quai Watier, 78400 Chatou, France

ABSTRACT

A variational approach is used to derivate a set of Serre equations for fully nonlinear, dispersive waves in channels of arbitrary cross-section. A family of travelling waves is found, as well as the relation between amplitude and celerity of solitary waves. An upper bound is proposed for the solitary wave amplitude as a function of the Froude number in trapezoidal cross-sectional canals, showing good agreement with an existing theory. For waves of moderate amplitude, cnoidal waves result with a soliton limit; the latter waves and their properties (celerity, wave number) are written as functions of the channel bank slope and channel bank curvature. The theoretical findings are in agreement with well-established results of the literature, in particular with more recent Boussinesq-type theories. A validation is proposed against existing experimental data.

INTRODUCTION

Aim of present work

Dispersive, non linear waves can occur in rivers and channels in many circumstances, like vessel wave wakes, waves due to ship lock or hydropower dam operations, to cite a few. Weakly dispersive, non linear wave trains, also referred to as undular bores, take place under various conditions like tidal bores (Chanson 2011) or Favre waves (Favre 1935). Understanding and modelling the behavior of these channel waves are thus necessary to the engineering design of river waterworks, canal operations or maintenance. Of particular interest is the example of Favre waves, due to rapid gate closure in hydropower stations (see Figure 1). These wave trains propagate far upstream with

little dissipation or damping, as evidenced by on-site tests (Violeau 2022) and laboratory models (Treske 1994). They can cause unexpected loads or floods along an extended part of the channel banks. The issue of dam break prediction is also at stake, recent numerical models showing that their numerical simulation benefit from dispersive wave models (see *e.g.* Mohapatra et al. 1999, Mohapatra and Chaudhry 2004 for an illustration with a Boussinesq-type model). Flow over weirs are also concerned, as demonstrated by Castro-Orgaz et al. (2022). More generally, for all channel dispersive, non linear waves, both the theory and the numerical modeling (and, to less extent, the design of scale models) require building relevant systems of equations.

In the context of the physical understanding and numerical modeling of non-linear, dispersive water waves, the Serre equations (Serre 1953a, Serre 1953b), also celebrated as the Serre–Green–Naghdi or Su–Gardner equations (Green et al. 1974, Su and Gardner 1969), have the advantage of being fully non-linear (through only weakly dispersive), contrary to the family of Boussinesq-type models. The Serre equations have been the subject of further extensions, including two-dimensional flow on arbitrary bottoms (Green and Naghdi 1976, Seabra-Santos et al. 1987). Only few papers (to the author's knowledge) refer to an extension of the Serre equations to channel flows with arbitrary channel cross section. A recent attempt was made by Debyaoui and Ersoy (2020) using the traditional asymptotic expansion method, leading to a complex formulation after long computations.

More generally, non-linear, dispersive waves in channels of arbitrary cross section have been the topic of limited publications so far, the prominent theoretical works being those by Peters (1968), Peregrine (1968), Fenton (1973), and more recently Teng and Wu (1997) and Winckler and Liu (2015). All these authors propose Boussinesq-like models and derive some propagation properties of classical wave families, i.e. cnoidal and solitary waves. In all these works the effect of the channel cross-sectional shape on these waves is primarily governed by the channel bank slope. As for numerical models of dispersive waves in arbitrary cross section channels, the Serre–Green–Naghdi equations are mostly considered, which requires a two-dimensional model (Chassagne et al. 2019, Biswas et al. 2021).

The present work aims at establishing simple, one-dimensional Serre-like equations for arbitrary cross-section channels with limited mathematical calculations. For this purpose, consider the variational approach by Clamond and Dutykh (2012). After building these equations we exhibit some families of travelling waves whose properties are successfully compared with those from the existing literature. The plan of the paper is as follows: after summarising Clamond and Dutykh's method (2012) in the next section, a first part is dedicated to the construction of an appropriate wave Lagrangian, which is then applied to channel flow to derive the Saint-Venant equations, then the newly proposed Serre model. In a second part we study travelling waves emerging from this model, with a focus on moderate amplitude waves for which a quantitative study is possible.

Clamond and Dutykh's wave Lagrangian

We consider Clamond and Dutykh (2012)'s variational approach, where they build shallow water wave equations from a variational approach for a potential, incompressible flow. To this purpose, they consider Luke's wave Lagrangian (1967):

$$\mathscr{L} = \int_t \int_{\mathbf{x}} \mathcal{L} d\mathbf{x} \mathrm{d}t, \tag{1}$$

$$\mathcal{L} = -\int_{-d}^{\eta} \left[gz + \phi_t + \tfrac{1}{2} |\nabla \phi|^2 + \tfrac{1}{2} \phi_z^2 \right] \mathrm{d}z, \tag{2}$$

where subscripts refer to partial derivatives. The flow potential is denoted as ϕ, the vertical coordinate is treated separately from the horizontals $\mathbf{x} = (x, y)^T$ and $\nabla (\cdot) = (\cdot)_{\mathbf{x}}$. Time is denoted as t, and the sea (or river, etc.) bottom is at $z = -d(\mathbf{x}, t)$ while $z = \eta(\mathbf{x}, t)$ represents the free surface elevation, so that the local water depth is $h = \eta + d$. Luke (1967) showed how the variation of the above Lagrangian leads to the equations of a free surface, incompressible potential flow. Clamond and Dutykh (2012) proposed to modify Luke's Lagrangian (1)–(2) to yield a *relaxed* form. To do so, they explicitely introduced the velocity $(\mathbf{u}, w)$ (with horizontal and vertical components $\mathbf{u}$ and w), as well as the potential flow condition $(\mathbf{u}, w) = (\nabla \phi, \phi_z)$, prescribed by a field of Lagrange

multipliers (λ, ν):

$$\begin{aligned}\mathcal{L} &= \hat{\phi}\eta_t + \check{\phi}d_t - \tfrac{1}{2}g\left(\eta^2 - d^2\right) \\ &\quad - \int_{-d}^{\eta}\left(\tfrac{1}{2}\left|\mathbf{u}\right|^2 + \tfrac{1}{2}w^2 + \lambda\cdot\left(\nabla\phi - \mathbf{u}\right) + \nu\left(\phi_z - w\right)\right)\mathrm{d}z,\end{aligned} \tag{3}$$

where the term gz was integrated explicitely, while ϕ_t was integrated by parts. In (3) and everywhere in this paper, we denote by $\hat{\varphi} = \varphi\left(z = \eta\right)$ and $\check{\varphi} = \varphi\left(z = -d\right)$ the values of an arbitrary field φ at the surface and the bottom, respectively. The resulting Lagrangian contains more unknowns but allows for more flexibility, hence the name of *relaxed* Lagrangian. Equation (3) is once more modified by the use of the following identities which assume vanishing fields for infinite values of the coordinates:

$$\int_{\mathbf{x}}\int_{-d}^{\eta}\lambda\cdot\nabla\phi\mathrm{d}z\mathrm{d}\mathbf{x} = \int_{\mathbf{x}}\int_{-d}^{\eta}\left(\nabla\cdot\left(\phi\lambda\right) - \phi\nabla\cdot\lambda\right)\mathrm{d}z\mathrm{d}\mathbf{x}, \tag{4}$$

then

$$\begin{aligned}\int_{\mathbf{x}}\int_{-d}^{\eta}\nabla\cdot\left(\phi\lambda\right)\mathrm{d}z\mathrm{d}\mathbf{x} &= \int_{\mathbf{x}}\left(\nabla\cdot\int_{-d}^{\eta}\phi\lambda dz - \hat{\phi}\hat{\lambda}\cdot\nabla\eta - \check{\phi}\check{\lambda}\cdot\nabla d\right)\mathrm{d}\mathbf{x} \\ &= -\int_{\mathbf{x}}\left(\hat{\phi}\hat{\lambda}\cdot\nabla\eta + \check{\phi}\check{\lambda}\cdot\nabla d\right)\mathrm{d}\mathbf{x},\end{aligned} \tag{5}$$

and finally

$$\int_{-d}^{\eta}\nu\phi_z dz = \hat{\nu}\hat{\phi} - \check{\nu}\check{\phi} - \int_{-d}^{\eta}\nu_z\phi\mathrm{d}z. \tag{6}$$

With (3) to (6), we obtain Clamond and Dutykh's Lagrangian:

$$\begin{aligned}\mathcal{L} &= \hat{\phi}\left(\eta_t + \hat{\lambda}\cdot\nabla\eta - \hat{\nu}\right) + \check{\phi}\left(d_t + \check{\lambda}\cdot\nabla d + \check{\nu}\right) - \tfrac{1}{2}g\left(\eta^2 - d^2\right) \\ &\quad + \int_{-d}^{\eta}\left(\lambda\cdot\mathbf{u} + \nu w - \tfrac{1}{2}\left|\mathbf{u}\right|^2 - \tfrac{1}{2}w^2 + \phi\left(\nabla\cdot\lambda + \nu_z\right)\right)\mathrm{d}z.\end{aligned} \tag{7}$$

Note that the surface and bottom potentials, $\hat{\phi}$ and $\check{\phi}$, are now the Lagrange multipliers of the kinematic boundary conditions of these two boundaries, applied to the conjugate velocity field (λ, ν), while ϕ is the multiplier associated to the incompressibility condition of the latter field.

VARIATIONAL DISPERSIVE WAVE MODEL FOR CHANNELS AND RIVERS

General considerations

We consider a channel or river of weak curvature, so that a one-dimensional approach is relevant. For the sake of generality we allow the bed/banks to be mobile, to account for sediment mobility, landslide, seism, etc. We assume the bed to have an average upstream-downstream slope of angle Θ with the horizontal, and place ourselves in a frame where the longitudinal axis x is inclined with the same angle, which allows accounting for the effects of a local bed slope d_x (see Figure 2). This amounts to changing g for $g\cos\Theta$, a horizontal driving force being added to the momentum equation. Extending Clamond and Dutykh's method to this framework is done by reducing the space integration of the Lagrangian to the x axis:

$$\mathscr{L} = \int_t \int_x \mathcal{L} \mathrm{d}x\mathrm{d}t, \tag{8}$$

while the Lagrangian density $\mathcal{L}$ is the integral of (7) on the transverse horizontal axis y, with the above-mentioned modifications:

$$\begin{aligned} \mathcal{L} \;=\; & \int_{-B^l}^{B^r} \left(\begin{array}{c} \hat{\phi}\left(\eta_t + \hat{\lambda}\eta_x + \hat{\mu}\eta_y - \hat{\nu}\right) + \check{\phi}\left(d_t + \check{\lambda}d_x + \check{\mu}d_y + \check{\nu}\right) \\ -\frac{1}{2}\left(g\cos\Theta\right)\left(\eta^2 - d^2\right) \end{array} \right) \mathrm{d}y \\ & + \int_{-B^l}^{B^r} \int_{-d}^{\eta} \left(\begin{array}{c} \left(g\sin\Theta\right)x + \lambda u + \mu v + \nu w - \frac{1}{2}\left(u^2 + v^2 + w^2\right) \\ +\phi\left(\lambda_x + \mu_y + \nu_z\right) \end{array} \right) \mathrm{d}z\mathrm{d}y \end{aligned} \tag{9}$$

where $y = -B^l(x,t)$ and $y = B^r(x,t)$ denote the transverse coordinates of the left and right banks, respectively; they both depend on the free surface elevation on banks. We decomposed the horizontal velocity and its conjugate field as $\mathbf{u} = u\mathbf{e}_x + v\mathbf{e}_y$ and $\lambda = \lambda\mathbf{e}_x + \mu\mathbf{e}_y$.

As explained by Clamond and Dutykh (2012), prescribing appropriate Ansätze for the velocity components and prescribing various kinds of boundary conditions in their Lagrangian allows finding various wave model equations. First, the Lagrangian (9) simplifies by assuming the potential to be

116 independent of the altitude z, *i.e.* $\phi = [\phi]\,(x,y,t)$. With this assumption, indeed:

$$\int_{-B^l}^{B^r}\left(\hat{\mu}\eta_y + \check{\mu}d_y + \int_{-d}^{\eta}\mu_y \mathrm{d}z\right)\mathrm{d}y = \int_{-B^l}^{B^r}\left(\int_{-d}^{\eta}\mu \mathrm{d}z\right)_y \mathrm{d}y \tag{10}$$

118 $$= \left[\int_{-d}^{\eta}\mu \mathrm{d}z\right]_{y=-B^l}^{y=B^r} = 0,$$

119 $$-\hat{\nu} + \check{\nu} + \int_{-d}^{\eta}\nu_z \mathrm{d}z = 0. \tag{11}$$

120 To establish (10), we used Leibnitz' integration rule, noting that $\eta + d = h = 0$ for $y = -B^l$ and
121 $y = B^r$. With the above two equations, we obtain

122 $$\mathcal{L} = \int_{-B^l}^{B^r}\left([\phi]\left(h_t + \hat{\lambda}\eta_x + \check{\lambda}d_x\right) - \tfrac{1}{2}\left(g\cos\Theta\right)\left(\eta^2 - d^2\right)\right)\mathrm{d}y \tag{12}$$

123 $$+\int_{-B^l}^{B^r}\int_{-d}^{\eta}\left(\left(g\sin\Theta\right)x + \lambda u + \mu v + \nu w - \tfrac{1}{2}\left(u^2+v^2+w^2\right) + [\phi]\,\lambda_x\right)\mathrm{d}z\mathrm{d}y.$$

124 note that $\hat{\nu}$, $\check{\nu}$, $\hat{\lambda}$ and $\check{\lambda}$ have been eliminated from the list of unknowns. In what follows, square
125 brackets will refer to vertical averaging; tilde will represent free-surface transverse averaging, and
126 an overbar will refer to the same average taken on the non-perturbed free-surface:

127 $$[\varphi]\,(x,y,t) \doteqdot \frac{1}{h\,(x,y,t)}\int_{-d(x,y,t)}^{\eta(x,y,t)}\varphi\,(x,y,z,t)\,\mathrm{d}z, \tag{13}$$

128 $$\widetilde{\varphi}\,(x,z,t) \doteqdot \frac{1}{B\,(x,t)}\int_{-B^l}^{B^r}\varphi\,(x,y,z=\eta\,(x,y,t)\,,t)\,\mathrm{d}y, \tag{14}$$

129 $$\overline{\varphi}\,(x,z,t) \doteqdot \frac{1}{B_0\,(x)}\int_{-B_0^l}^{B_0^r}\varphi\,(x,y,z=0,t)\,\mathrm{d}y, \tag{15}$$

130 where $B\,(x,t) = B^l\,(x,t) + B^r\,(x,t)$ is the surface width and $B_0\,(x) = B_0^l\,(x) + B_0^r\,(x)$ its value in
131 the absence of wave (Figure 2), the rest water level being $z = 0$. Applying the first two averages
132 defines the section-average:

133 $$\langle\varphi\rangle\,(x,t) \doteqdot \frac{1}{A\,(x,t)}\int_A \varphi\,(x,y,z,t)\,\mathrm{d}y\mathrm{d}z = \widetilde{[\varphi]}\,(x,t)\,, \tag{16}$$

where $A\left(x,t\right)$ is the wetted area:

$$A\left(x,t\right) \doteq \int_{-B^l}^{B^r} h\left(x,y,t\right) \mathrm{d}y = B\left(x,t\right) \tilde{h}\left(x,t\right). \tag{17}$$

Like the bank sides, A and B explicitly depend on the free surface elevation $\eta\left(x,y,t\right)$. At rest, the section is denoted as $A_0\left(x\right) = B_0\left(x\right) \bar{d}\left(x\right)$, with $\bar{d}\left(x\right)$ as the rest width-averaged depth.

Further, we impose the potential as constant on the whole channel cross section, *i.e.* $\phi = \langle\phi\rangle\left(x,t\right)$. This suggests that the longitudinal velocity and its conjugate obey the same rule: $u = \langle u\rangle\left(x,t\right)$ and $\lambda = \langle\lambda\rangle\left(x,t\right)$, so that (12) reads

$$\begin{aligned}
\mathcal{L} \;=\; & \langle\phi\rangle \left(\int_{-B^l}^{B^r} h_t \mathrm{d}y + \int_{-B^l}^{B^r} \left(\langle\lambda\rangle h\right)_x \mathrm{d}y \right) \\
& -\tfrac{1}{2}\left(g\cos\Theta\right) \int_{-B^l}^{B^r} \left(\eta^2 - d^2\right) \mathrm{d}y + A\left(\left(g\sin\Theta\right) x + \langle\lambda\rangle\langle u\rangle - \tfrac{1}{2}\langle u\rangle^2 \right) \\
& + \int_{-B^l}^{B^r} \int_{-d}^{\eta} \left(\mu v + \nu w - \tfrac{1}{2}\left(v^2 + w^2\right) \right) \mathrm{d}z\mathrm{d}y.
\end{aligned} \tag{18}$$

However, since h vanishes on the banks, the Leibnitz' rule gives

$$\begin{aligned}
\int_{-B^l}^{B^r} h_t \mathrm{d}y \;&=\; \left(\int_{-B^l}^{B^r} h \mathrm{d}y \right)_t = A_t, \\
\int_{-B^l}^{B^r} \left(\langle\lambda\rangle h\right)_x \mathrm{d}y \;&=\; \left(\langle\lambda\rangle \int_{-B^l}^{B^r} h \mathrm{d}y \right)_x = \left(A\langle\lambda\rangle\right)_x,
\end{aligned} \tag{19}$$

therefore

$$\begin{aligned}
\mathcal{L} \;=\; & \langle\phi\rangle \left(A_t + \left(A\langle\lambda\rangle\right)_x\right) - \tfrac{1}{2}\left(g\cos\Theta\right) \int_{-B^l}^{B^r} \left(\eta^2 - d^2\right) \mathrm{d}y \\
& + A\left(\left(g\sin\Theta\right) x + \langle\lambda\rangle\langle u\rangle - \tfrac{1}{2}\langle u\rangle^2 \right) \\
& + \int_{-B^l}^{B^r} \int_{-d}^{\eta} \left(\mu v + \nu w - \tfrac{1}{2}\left(v^2 + w^2\right) \right) \mathrm{d}z\mathrm{d}y.
\end{aligned} \tag{20}$$

In what follows, we will use the Lagrangian (20) to derive Serre-like equations for arbitrary cross-sectional channels.

One dimensional Saint-Venant equations

We start by checking that the Lagrangian (20) yields the one-dimensional Saint-Venant equations in arbitrary cross-sectional channels when no additional condition is imposed, as it does in two dimensions on a flat bed, as explained by (Clamond and Dutykh 2012). The Serre equations studied later are an extension of the Saint-Venant equations, which are relevant for non linear but *non dispersive* waves.

The variations of $\mathcal{L}$ with respect to $\langle\phi\rangle$, $\langle u\rangle$ and $\langle\lambda\rangle$ give

$$\frac{\delta\mathcal{L}}{\delta\langle\phi\rangle} = A_t + \left(A\langle\lambda\rangle\right)_x, \tag{21}$$

$$\frac{\delta\mathcal{L}}{\delta\langle u\rangle} = A\left(\langle\lambda\rangle - \langle u\rangle\right), \tag{22}$$

$$\frac{\delta\mathcal{L}}{\delta\langle\lambda\rangle} = A\left(-\langle\phi\rangle_x + \langle u\rangle\right), \tag{23}$$

(integration by parts of $\langle\phi\rangle\left(A\langle\lambda\rangle\right)_x$ have been used to calculate the last line). Cancelling the above lines shows that the flow is potential while $\langle\lambda\rangle = \langle u\rangle = \langle\phi\rangle_x$, and (21) is the continuity equation:

$$A_t + \left(A\langle u\rangle\right)_x = 0. \tag{24}$$

Cancelling the variation of $\mathcal{L}$ with respect to v, μ, w, ν (which remain unknown functions) leads to

$$\int_{-B^l}^{B^r}\int_{-d}^{\eta}\left(v\delta\mu + (\mu - v)\,\delta v + w\delta\nu + (\nu - w)\,\delta w\right)\mathrm{d}z\mathrm{d}y = 0, \tag{25}$$

regardless of the variations $\delta\mu$, δv, $\delta\nu$ and δw, which gives $\mu = v = \nu = w = 0$. Hence, under the present assumptions the flow is purely longitudinal: dispersive waves, which rely on the existence of vertical velocity, will require more than the present approach. Finally, cancelling the variation of $\mathcal{L}$ with respect to η necessitates writting the variation of the cross sectional area:

$$\delta A = \delta\int_{-B^l}^{B^r} h\mathrm{d}y = \int_{-B^l}^{B^r}\delta\eta\mathrm{d}y, \tag{26}$$

which holds because h vanishes on the banks. The same reasoning is used to calculate the variation of the integral of $\eta^2 - d^2$ in (20). Using integration by parts, we obtain

$$\left(- \langle \phi \rangle_t - \tfrac{1}{2} \langle u \rangle^2 + (g \sin \Theta)\, x \right) \int_{-B^l}^{B^r} \delta\eta \mathrm{d}y - (g \cos \Theta) \int_{-B^l}^{B^r} \eta \delta\eta \mathrm{d}y = 0. \tag{27}$$

This being true for all variations $\delta\eta$, we find

$$\langle \phi \rangle_t + \tfrac{1}{2} \langle u \rangle^2 + (g \cos \Theta)\, \eta = (g \sin \Theta)\, x. \tag{28}$$

As a conclusion, we have $\eta = \tilde{\eta}$: the free surface elevation does not depend on y (it is invariant along the channel width), and (26) reads

$$A_{\tilde{\eta}} = B. \tag{29}$$

Taking the gradient of (28) leads to the momentum equation:

$$\langle u \rangle_t + \langle u \rangle \langle u \rangle_x + (g \cos \Theta)\, \tilde{\eta}_x = g \sin \Theta. \tag{30}$$

Using the continuity equation (24), one can write it in the well-known conservative form:

$$(A \langle u \rangle)_t + \left(A \langle u \rangle^2 + (g \cos \Theta)\, I \right)_x = (g \sin \Theta)\, A + (g \cos \Theta)\, J, \tag{31}$$

where we made use of the following definitions:

$$I(h) \doteqdot \tfrac{1}{2} \int_{-B^l}^{B^r} h^2 \mathrm{d}y = \tfrac{1}{2} B \widetilde{h^2}, \tag{32}$$

$$J(h) \doteqdot \int_{-B^l}^{B^r} h d_x \mathrm{d}y = B \widetilde{h d_x}, \tag{33}$$

(which gives $I_x = A\tilde{\eta}_x + J$, using (29)). We observe that

$$(g \sin\Theta)\, A + (g \cos\Theta)\, J = g \int_{-B^l}^{B^r} h\, (\sin\Theta - d_x \cos\Theta)\, \mathrm{d}y \tag{34}$$

is a purely geometrical source term, modeling the effects of global ($\sin\Theta$) and local ($d_x \cos\Theta$) bed slope along the longitudinal axis. The above equations are classical and widely used in understanding channel flows as long as the pressure remains almost hydrostatic, *i.e.*, for long waves or breaking bores. Additional terms will allow modeling weakly dispersive (*i.e.*, shorter) waves in what follows.

Arbitrary cross sectional Serre equations

As shown by (Clamond and Dutykh 2012) in two dimensions on a flat bed, the Serre equations are obtained from the same Lagrangian than the Saint-Venant equations, by prescribing the kinematic free surface boundary condition through the conjugate velocity field. This requires an Ansatz for the vertical velocity and one for its conjugate field. Following (Clamond and Dutykh 2012), we set

$$w = \frac{z+d}{\eta+d}\hat{w}, \tag{35}$$

$$v = \frac{z+d}{\eta+d}\hat{v}, \tag{36}$$

where $\hat{w}\,(x,y,t)$ and $\hat{v}\,(x,y,t)$ are their values on the free surface, and we impose $\hat{v} = \eta_t + \langle\lambda\rangle\,\eta_x + \hat{\mu}\eta_y$. the Lagrangian (20) now becomes

$$\begin{aligned}\mathcal{L} = {} & \langle\phi\rangle\,(A_t + (A\,\langle\lambda\rangle)_x) - \tfrac{1}{2}\,(g\cos\Theta)\int_{-B^l}^{B^r}\left(\eta^2 - d^2\right)\mathrm{d}y \\ & + A\left((g\sin\Theta)\,x + \langle\lambda\rangle\,\langle u\rangle - \tfrac{1}{2}\,\langle u\rangle^2\right) + \int_{-B^l}^{B^r}\int_{-d}^{\eta}\left(\mu v - \tfrac{1}{2}v^2\right)\mathrm{d}z\mathrm{d}y \\ & + \int_{-B^l}^{B^r} h\left(\tfrac{1}{3}\left(\eta_t + \langle\lambda\rangle\,\eta_x + \hat{\mu}\eta_y\right)\hat{w} - \tfrac{1}{6}\hat{w}^2\right)\mathrm{d}y.\end{aligned} \tag{37}$$

In dispersive channel waves and bores, it is known that the free surface elevation depends on the transverse direction y (Peregrine (1969), Treske (1994), Teng and Wu (1997)). However, in

the present study we will neglect this phenomenon, which is not compatible with our Ansätze (35)–(36). Therefore, if we further ignore transverse variations of all quantities of interest, *i.e.* $\eta = \tilde{\eta}, \hat{\mu} = \widetilde{\hat{\mu}}, \hat{v} = \widetilde{\hat{v}}, \hat{w} = \widetilde{\hat{w}}$, this gives

$$\begin{aligned} \mathcal{L} &= \langle\phi\rangle \left(A_t + \left(A\langle\lambda\rangle\right)_x\right) - \tfrac{1}{2}\left(g\cos\Theta\right)\int_{-B^l}^{B^r}\left(\tilde{\eta}^2 - d^2\right)\mathrm{d}y \\ &+A\left(\begin{array}{c}\left(g\sin\Theta\right)x + \langle\lambda\rangle\langle u\rangle - \frac{1}{2}\langle u\rangle^2 \\ +\frac{1}{3}\left(\widetilde{\hat{\mu}}\widetilde{\hat{v}} + \left(\tilde{\eta}_t + \langle\lambda\rangle\tilde{\eta}_x\right)\widetilde{\hat{w}} - \frac{1}{2}\left(\widetilde{\hat{v}}^2 + \widetilde{\hat{w}}^2\right)\right)\end{array}\right). \end{aligned} \tag{38}$$

Cancelling the variation of this Lagrangian with respect to $\langle\phi\rangle$ and $\langle u\rangle$ gives $\langle\lambda\rangle = \langle u\rangle$ and $A_t + \left(A\langle u\rangle\right)_x = 0$, as above. Cancelling the variations with repect to $\widetilde{\hat{\mu}}$, $\widetilde{\hat{v}}$, $\widetilde{\hat{w}}$ and $\langle\lambda\rangle$ leads to

$$\widetilde{\hat{\mu}} = \widetilde{\hat{v}} = 0, \tag{39}$$

$$\widetilde{\hat{w}} = \tilde{\eta}_t + \langle u\rangle\tilde{\eta}_x, \tag{40}$$

$$\langle\phi\rangle_x = \langle u\rangle + \tfrac{1}{3}\tilde{\eta}_x\widetilde{\hat{w}}. \tag{41}$$

Therefore, the transverse velocity and its conjugate cancel out and the kinematic boundary condition at the free surface is satisfied as expected. On the other hand, the flow is no longer potential, as shown by (41). The variation of $\mathcal{L}$ with respect to $\tilde{\eta}$ gives

$$\langle\phi\rangle_t + \tfrac{1}{2}\langle u\rangle^2 + \left(g\cos\Theta\right)\tilde{\eta} = \left(g\sin\Theta\right)x - \tfrac{1}{3}\left(\tilde{h}\left(\widetilde{\hat{w}}_t + \langle u\rangle\widetilde{\hat{w}}_x\right) + \langle u\rangle\widetilde{\hat{w}}\tilde{\eta}_x - \tfrac{1}{2}\widetilde{\hat{w}}^2\right). \tag{42}$$

Taking its gradient with (40)–(41) and applying a few manipulations leads to

$$\langle u\rangle_t + \langle u\rangle\langle u\rangle_x + \left(g\cos\Theta\right)\tilde{\eta}_x = g\sin\Theta - \tfrac{1}{3}\left(\left(\tilde{h}\left(\widetilde{\hat{w}}_t + \langle u\rangle\widetilde{\hat{w}}_x\right)\right)_x + \tilde{\eta}_x\left(\widetilde{\hat{w}}_t + \langle u\rangle\widetilde{\hat{w}}_x\right)\right). \tag{43}$$

On the other hand, with (29) we have

$$A_x\tilde{h} = A\tilde{\eta}_x + \tilde{h}\int_{-B^l}^{B^r} d_x\mathrm{d}y, \tag{44}$$

which allows for writing the conservative form of the momentum equation (43) as follows:

$$\begin{aligned} (A\langle u\rangle)_t &+ \left(A\langle u\rangle^2 + (g\cos\Theta)\, I + \tfrac{1}{3}A\tilde{h}\left(\widetilde{\hat{w}}_t + \langle u\rangle\,\widetilde{\hat{w}}_x\right)\right)_x \\ &= (g\sin\Theta)\, A - (g\cos\Theta)\, J + \tfrac{1}{3}\tilde{h}\left(\widetilde{\hat{w}}_t + \langle u\rangle\,\widetilde{\hat{w}}_x\right)\int_{-B^l}^{B^r} d_x \mathrm{d}y. \end{aligned} \tag{45}$$

As for the Saint-Venant equations, the right-hand side vanishes on a flat bed. Equation (45) is a Serre-like momentum equation generalised to arbitrary cross section channels. We see that the additional terms with respect to the section-averaged Saint-Venant momentum equation (31) depend on the vertical velocity at the free surface, thus on the non-hydrostaticity of the pressure field. With the above findings, the Lagrangian (38) is simplified to

$$\mathcal{L}\left(\tilde{\eta}, \langle u\rangle\right) = A\left(-\tfrac{1}{2}\left(g\cos\Theta\right)\left(\tilde{h} - 2\tilde{d}\right) + \left(g\sin\Theta\right)x + \tfrac{1}{2}\langle u\rangle^2 + \tfrac{1}{6}\left(\tilde{\eta}_t + \langle u\rangle\,\tilde{\eta}_x\right)^2\right). \tag{46}$$

The Lagrangian being time-independent, Noether's theorem states the conservation of an energy in the absence of external forcing, *i.e.*, when the bed is horizontal and fixed. A general energy conservation equation stems from (43) and (45) along with the continuity equation, by noting that

$$A_t = B\tilde{\eta}_t + \int_{-B^l}^{B^r} d_t \mathrm{d}y, \tag{47}$$

$$I_t = A\tilde{\eta}_t + \int_{-B^l}^{B^r} h d_t \mathrm{d}y. \tag{48}$$

After a few manipulations, we obtain

$$\begin{aligned} &\left(A\left(\tfrac{1}{2}\langle u\rangle^2 + \tfrac{1}{6}\widetilde{\hat{w}}^2\right) + \tfrac{1}{2}\left(g\cos\Theta\right)\left(\tilde{\eta}^2 - \widetilde{d^2}\right)\right)_t \\ &+ \left(A\langle u\rangle\left(\tfrac{1}{2}\langle u\rangle^2 + \tfrac{1}{6}\widetilde{\hat{w}}^2 + (g\cos\Theta)\,\tilde{\eta} + \tfrac{1}{3}\tilde{h}\left(\widetilde{\hat{w}}_t + \langle u\rangle\,\widetilde{\hat{w}}_x\right)\right)\right)_x \\ &= (g\sin\Theta)\, A\langle u\rangle - (g\cos\Theta)\int_{-B^l}^{B^r} h d_t \mathrm{d}y - \tfrac{1}{3}\tilde{h}\left(\widetilde{\hat{w}}_t + \langle u\rangle\,\widetilde{\hat{w}}_x\right)\int_{-B^l}^{B^r} d_t \mathrm{d}y. \end{aligned} \tag{49}$$

In what follows, consider special cases where the channel is straight, flat and prismatic ($\Theta = d_x =$

$d_t = 0$). Under these assumptions, (45) simplifies and the final system, with the continuity equation and (40), is

$$A_t + (A\langle u\rangle)_x = 0, \tag{50}$$

$$(A\langle u\rangle)_t + \left(A\langle u\rangle^2 + \tfrac{1}{2}gB\widetilde{h^2} + \tfrac{1}{3}A\tilde{h}\left(\widetilde{\hat{w}}_t + \langle u\rangle\,\widetilde{\hat{w}}_x\right)\right)_x = 0, \tag{51}$$

$$\widetilde{\hat{w}} = \tilde{\eta}_t + \langle u\rangle\,\tilde{\eta}_x, \tag{52}$$

with the following energy conservation law:

$$\begin{aligned}&\left(A\left(\tfrac{1}{2}\langle u\rangle^2 + \tfrac{1}{6}\widetilde{\hat{w}^2}\right) + \tfrac{1}{2}gB(\tilde{\eta}^2 - \widetilde{d^2})\right)_t \\ &+ \left(A\langle u\rangle\left(\tfrac{1}{2}\langle u\rangle^2 + \tfrac{1}{6}\widetilde{\hat{w}^2} + g\tilde{\eta} + \tfrac{1}{3}\tilde{h}\left(\widetilde{\hat{w}}_t + \langle u\rangle\,\widetilde{\hat{w}}_x\right)\right)\right)_x = 0.\end{aligned} \tag{53}$$

Equations (50)–(52) and (53) reduce to the ordinary Serre equations on a flat bed (see, *e.g.*, (Clamond et al. 2017) for the rectangular channel section.

TRAVELLING WAVES IN UNIFORM CHANNELS

We are now interested in a family of waves that is sometimes encountered in channel engineering: travelling waves, *i.e.*, that propagate with a constant celerity with a constant shape. Consider a wave travelling in a channel satisfying the assumptions that led to the system (50)–(52). We seek for all quantities as functions of $\xi \doteqdot x - ct$, c being the unknown celerity. Defining $U \doteqdot \langle u\rangle - c$, (52) reads $\widetilde{\hat{w}} = U\tilde{\eta}'$ and the other two equations read

$$(AU)' = 0, \tag{54}$$

$$\left(AU\,(U+c) + \tfrac{1}{2}gB\widetilde{h^2} + \tfrac{1}{3}A\tilde{h}U\,(U\tilde{\eta}')'\right)' = 0, \tag{55}$$

the prime denoting the derivation with respect to ξ. We will now investigate the solutions of the latter system.

General solution

Integrating (54) and (55) once gives

$$AU = -\left(1-\bar{C}_0\right) A_0 c, \tag{56}$$

$$AU\,(U+c) + \tfrac{1}{2} g\left(B\widetilde{h^2} - B_0\overline{d^2}\right) + \tfrac{1}{3} A\tilde{h} U\,(U\tilde{\eta}')' = \bar{C}_1, \tag{57}$$

where $\bar{C}_0, \bar{C}_1$ are two constants that vanish in the absence of waves. Their values will determine the type of wave at stake. Observing that $A' = B\tilde{\eta}'$ and $\tilde{h} = \frac{A}{B}$, the second term in (57), after multiplication by $\frac{A'}{A^2}$, is integrated as follows:

$$\int \left(B\widetilde{h^2} - B_0\overline{d^2}\right)\frac{B}{A^2}\mathrm{d}\tilde{\eta} = \int \frac{\widetilde{h^2}}{\tilde{h}^2}\mathrm{d}\tilde{\eta} + \frac{B_0\overline{d^2}}{A}. \tag{58}$$

We now define the dimensionless free surface elevation and channel section as

$$\mathcal{N} \doteq \frac{\tilde{\eta}}{\overline{d}}, \tag{59}$$

$$\mathcal{A}(\mathcal{N}) \doteq \frac{A}{A_0}.$$

After manipulations, it is found that

$$\int_0^{\mathcal{N}} \frac{\widetilde{h^2}\,(n)}{\tilde{h}^2\,(n)}\mathrm{d}n = 2\mathcal{N} + \frac{1}{\overline{d}}\left(\frac{\overline{d^2}}{\overline{d}} - \frac{\widetilde{h^2}\,(\mathcal{N})}{\tilde{h}\,(\mathcal{N})}\right) = \frac{\overline{d^2}}{\overline{d}^2} - \frac{\frac{\widetilde{d^2}(\mathcal{N})}{\overline{d}^2} - \mathcal{N}^2}{\frac{\tilde{d}(\mathcal{N})}{\overline{d}} + \mathcal{N}}, \tag{60}$$

n being a dummy variable. We now substitute U from (56) into (57), multiply the latter by $\frac{A'}{A^2}$ and integrate once more. Using (60), we obtain the free surface slope (squared) as a function of the free surface elevation:

$$\tfrac{1}{3}\left(\frac{\mathrm{d}\mathcal{N}}{\mathrm{d}\xi}\right)^2 = 1 - 2C_0\mathcal{A}(\mathcal{N}) + C_1\mathcal{A}^2(\mathcal{N}) - \frac{C_2}{\mathcal{F}_0^2}\mathcal{A}(\mathcal{N})\left(\frac{\overline{d^2}}{\overline{d}^2} - \mathcal{A}(\mathcal{N})\,\frac{\frac{\widetilde{d^2}(\mathcal{N})}{\overline{d}^2} - \mathcal{N}^2}{\frac{\tilde{d}(\mathcal{N})}{\overline{d}} + \mathcal{N}}\right), \tag{61}$$

C_0, C_1 being two constants linked to $\bar{C}_0, \bar{C}_1$, and $C_2 \neq 0$ another constant, while $\mathcal{F}_0$ is a Froude number:

$$\mathcal{F}_0 \doteq \frac{c}{\sqrt{g\overline{d}}}. \tag{62}$$

The latter ordinary differential equation can be written in separate form to give the general implicit solution as integral:

$$\frac{x-ct}{\overline{d}} = \pm\frac{1}{\sqrt{3}} \int \frac{\mathrm{d}\mathcal{N}}{\sqrt{1 - 2C_0\mathcal{A}\left(\mathcal{N}\right) + C_1\mathcal{A}^2\left(\mathcal{N}\right) - \frac{C_2}{\mathcal{F}_0^2}\mathcal{A}\left(\mathcal{N}\right)\left(\frac{\overline{d^2}}{\overline{d}^2} - \mathcal{A}\left(\mathcal{N}\right)\frac{\frac{\widetilde{d^2}(\mathcal{N})}{\overline{d}^2} - \mathcal{N}^2}{\frac{\tilde{d}(\mathcal{N})}{\overline{d}} + \mathcal{N}}\right)}}. \tag{63}$$

This is a 4–parameter family of solutions, which can in principle be integrated for a given cross section, *i.e.*, for particular values of $\overline{d}, \overline{d^2}$ and particular formulae for $\mathcal{A}\left(\mathcal{N}\right), \tilde{d}\left(\mathcal{N}\right), \widetilde{d^2}\left(\mathcal{N}\right)$. It is worth noting that the latter two integrals involve negative values of $d\left(x, y, t\right)$, for $-B^l \leqslant y < B_0^l$ and $B_0^r < y \leqslant B^r$ (see Figure 3 as an illustration).

A family of solitary waves is found for $(C_0, C_1, C_2) = (1, 1, 1)$. In this case, setting $\mathrm{d}\mathcal{N}/\mathrm{d}\xi = 0$ at the wave crest gives the solitary wave celerity c_s versus the dimensionless wave amplitude $\mathcal{N}^*$:

$$\frac{c_s}{\sqrt{g\overline{d}}} = \frac{\sqrt{\mathcal{A}\left(\mathcal{N}^*\right)\left(\frac{\overline{d^2}}{\overline{d}^2} - \mathcal{A}\left(\mathcal{N}^*\right)\frac{\frac{\widetilde{d^2}(\mathcal{N}^*)}{\overline{d}^2} - \mathcal{N}^{*2}}{\frac{\tilde{d}(\mathcal{N}^*)}{\overline{d}} + \mathcal{N}^*}\right)}}{\mathcal{A}\left(\mathcal{N}^*\right) - 1}. \tag{64}$$

For a rectangular section, the usual results are recovered: we have $\mathcal{A}\left(\mathcal{N}\right) = 1 + \mathcal{N}$, $\tilde{d}\left(\mathcal{N}\right) = \overline{d}$, $\widetilde{d^2}\left(\mathcal{N}\right) = \overline{d}^2$ and (64) gives

$$\frac{c_s}{\sqrt{g\overline{d}}} = \sqrt{1 + \mathcal{N}^*}, \tag{65}$$

according to Russell's experimental findings and Boussinesq's and Rayleigh's classical theories (see, *e.g.* Carter and Cienfuegos (2011)). This result, however, is less accurate than Teng and Wu's Boussinesq-type model (1992), according to Daily and Stephans' experiments (Daily and Stephans

1952). On the other hand, (63) now reads

$$\frac{x - c_s t}{\overline{d}} = \pm \frac{1}{\sqrt{3}} \int \frac{d\mathcal{N}}{\mathcal{N}\sqrt{1 - \frac{1}{\mathcal{F}_0^2}(1 + \mathcal{N})}}, \tag{66}$$

which is integrated to give the well-known solitary wave of the Serre equations (Serre 1953b):

$$\mathcal{N} = \mathcal{N}^* \operatorname{sech}^2\left(\frac{\sqrt{3\left(\mathcal{F}_0^2 - 1\right)}}{2\mathcal{F}_0} \frac{x - c_s t}{\overline{d}}\right), \tag{67}$$

$$\mathcal{N}^* \doteq \mathcal{F}_0^2 - 1. \tag{68}$$

Upper bound of the solitary wave amplitude

For practical reasons, it is interesting to predict an upper bound of wave elevation. As explained by Hager and Hutter (1984), this can be deduced from the hydraulic head. From the energy conservation equation (53), the head in the present model is given by

$$H = \frac{1}{2g}\langle u \rangle^2 + \frac{1}{6g}\widetilde{\hat{w}}^2 + \tilde{\eta} + \frac{1}{3g}\tilde{h}\left(\widetilde{\hat{w}}_t + \langle u \rangle \widetilde{\hat{w}}_x\right). \tag{69}$$

In the case of progressive waves, using $\widetilde{\hat{w}} = U\tilde{\eta}'$ gives the head in the moving frame (where the wave is steady) as

$$H = \tilde{\eta} + \frac{1}{2}\frac{c_s^2}{g}\left(\frac{A_0}{A}\right)^2\left(1 + \frac{1}{3}\left(2\tilde{h}\tilde{\eta}'' - \tilde{\eta}'^2\right)\right). \tag{70}$$

The second derivative $\tilde{\eta}''$ is deduced by differentiating (61). With the above definitions, lengthy but straightforward manipulations yields the head in the following simple form

$$H = \frac{1}{2}\mathcal{F}_0^2 \overline{d}, \tag{71}$$

confirming that the head is conserved. Now, following Hager and Hutter (1984), consider a solitary wave. The head in the moving frame must obviously satisfy $H \geq \tilde{\eta}^*$, which is the width-averaged

depth at the wave crest. Equation (71) thus yields

$$\tfrac{1}{2}\mathcal{F}_0^2\left(\mathcal{N}^*\right) \geqslant \mathcal{N}^*. \tag{72}$$

The Froude number being linked to the wave amplitude $\mathcal{N}^*$ by (64), this gives an implicit equation for the upper bound of the solitary wave amplitude $\mathcal{N}_c^*$:

$$\frac{\overline{d^2}}{\overline{d}^2} - \mathcal{A}\left(\mathcal{N}_c^*\right)\frac{\frac{\widetilde{d^2}\left(\mathcal{N}_c^*\right)}{\overline{d}^2} - \mathcal{N}_c^{*2}}{\frac{\tilde{d}\left(\mathcal{N}_c^*\right)}{\overline{d}} + \mathcal{N}_c^*} = \frac{2\mathcal{N}_c^*\left(1-\mathcal{A}\left(\mathcal{N}_c^*\right)\right)^2}{\mathcal{A}\left(\mathcal{N}_c^*\right)}. \tag{73}$$

Above the critical amplitude $\mathcal{N}_c^*$, waves should be unstable and break. However, as pointed out by Hager and Hutter (1984) instability may occur for smaller amplitudes, the above criterion being sufficient but not necessary. For the rectangular section (73) gives $\mathcal{N}_c^* = 1$, thus $\mathcal{F}_0 = \sqrt{2}$: the solitary wave amplitude cannot exceed the rest water depth, in agreement with Hager and Hutter (1984).

Trapezoidal cross section

Still following Hager and Hutter (1984), we now investigate the trapezoidal cross-sectional case, the most frequent in hydraulic civil engineering. Call b the width of the flat, horizontal part of the bed, h_0 the rest depth above the latter and $m = \cot\theta$ the bank slope (Figure 3), all quantities of interest can be written as functions of the following parameters:

$$\beta = m\frac{h_0}{b} \in \left[-\tfrac{1}{2}, +\infty\right), \tag{74}$$

$$\alpha = \frac{\beta\left(\beta+1\right)}{\left(2\beta+1\right)^2} \in \left(-\infty, \tfrac{1}{4}\right]. \tag{75}$$

For a solitary wave, equation (63) reads

$$\frac{x - c_s t}{\overline{d}} = \pm\frac{\mathcal{F}_0}{\sqrt{3}}\int \frac{\mathrm{d}\mathcal{N}}{\mathcal{N}\sqrt{\mathcal{F}_0^2\left(1+\alpha\mathcal{N}\right)^2 - \left(1+\mathcal{N}+\alpha\mathcal{N}^2\right)\left(1+\frac{4}{3}\alpha\mathcal{N}\right)}}, \tag{76}$$

and must be integrated by numerical means (the quadrature method is explained in the Supplementary Materials). Figure 4 shows three solitons with $\alpha = 0.25$ (triangular cross section) and wave amplitude $\mathcal{N}^* = 0.1, 0.2, 0.3$.

In practice, the above variables $(\mathcal{F}_0, \mathcal{N})$ may be replaced by Hager and Hutter (1984)'s notation $(f = \frac{Q^2}{gb^2h_0^3}, y = \frac{h}{h_0})$, where Q is the flowrate far upstream in the moving frame. They are linked to the present variables by

$$f = \frac{(1+\beta)^3}{1+2\beta}\mathcal{F}_0^2, \tag{77}$$

$$y = 1 + \frac{1+\beta}{1+2\beta}\mathcal{N}. \tag{78}$$

Cancelling the denominator in (76) gives the Froude number versus the wave amplitude as

$$\mathcal{F}_0^2 = \frac{\left(1+\mathcal{N}^*+\alpha\mathcal{N}^{*2}\right)\left(1+\frac{4}{3}\alpha\mathcal{N}^*\right)}{\left(1+\alpha\mathcal{N}^*\right)^2}, \tag{79}$$

which is also obtained from (64). Using (77)–(78) this can also be written

$$f = (1+\beta)^2\,\frac{y^*\left(1+\beta y^*\right)\left(2\beta+3+4\beta y^*\right)}{3\left(\beta+1+\beta y^*\right)^2}. \tag{80}$$

This is plotted on Figure 5, compared with Hager and Hutter (1984)'s model (their Figure 5; their model is summarised in the Supplementary Materials). One can see that the present model is close to Hager and Hutter (1984)'s; in particular, both models give, for small amplitude waves

$$f = \frac{(\beta+1)^3}{2\beta+1} + \frac{(\beta+1)^2\left(10\beta^2+10\beta+3\right)}{3\left(2\beta+1\right)^2}\left(y^*-1\right) + O\left(\left(y^*-1\right)^2\right). \tag{81}$$

Equation (73), giving the upper bound of the solitary wave amplitude, now reads

$$\mathcal{N}_c^{*3} + \frac{5}{2\alpha}\mathcal{N}_c^{*2} + \frac{3-4\alpha}{2\alpha^2}\mathcal{N}_c^* - \frac{3}{2\alpha^2} = 0, \tag{82}$$

with solution

$$\mathcal{N}_c^* = \Psi(\alpha) + \frac{\frac{2}{3\alpha} + \frac{7}{36\alpha^2}}{\Psi(\alpha)} - \frac{5}{6\alpha}, \tag{83}$$

where

$$\Psi(\alpha) = \left(\frac{5}{108\alpha^3} - \frac{1}{12\alpha^2} + \sqrt{-\frac{8}{27\alpha^3} - \frac{109}{432\alpha^4} - \frac{1}{12\alpha^5} - \frac{1}{192\alpha^6}} \right)^{1/3}. \tag{84}$$

Hager and Hutter (1984) explain how their model allows for writing an upper bound of the wave elevation above the bed y_c^* from the considerations repeated in the previous section. They do not exhibit all their formulae, but it is noteworthy that their model simplifies to

$$\frac{f(y^*)}{2(1+\beta)^2} \geqslant y^* - 1, \tag{85}$$

which is exactly equation (72) of the present model (that we proved above being valid for all cross-sectional shapes). However, Hager and Hutter (1984) obtained a different relation between the amplitude and the Froude number. With our model, (73) gives, for the trapezoidal section, an implicit equation connecting the upper bound of y^*, denoted as y_c^*, with the corresponding value of f:

$$2f\left(y_c^{*3} + 2y_c^{*2} - 3y_c^* - 3\right) + \sqrt{2f(y_c^* - 1)}\, y_c^* (y_c^* + 2)(4y_c^* - 5) + 2y_c^* (2y_c^* + 1)(y_c^* - 1)^2 = 0. \tag{86}$$

The above equation is a second order polynomial in $\sqrt{f}$, giving the bold solid line on Figure 5 (only values of y^* larger than 1 are represented, *i.e.*, positive waves). The rectangular section case $(f, y_c^*) = (2, 2)$ is recovered, while the asymptotic y_c^* value for large f (large β) is 0.4605. Therefore, the maximum solitary wave amplitude in very wide and shallow channels with bank slopes is bounded by $\tilde{\eta}_c^*(\beta \longrightarrow +\infty) = 0.4605 h_0$ (while $\tilde{\eta}_c^*(\beta = 0) = h_0$ in a rectangular section, as a reminder). The intersection of the curve (86) with the axis $f = 1$ is given by $\beta = -0.288$ and $y_c^* = 1.986$. The same Figure shows the critical wave elevation in Hager and Hutter (1984) (the detailed computations are summarized in the Supplementary Materials).

Cnoidal waves of moderate amplitude

Contrary to the case of rectangular section, in general the implicit solution (63) cannot be solved for the surface elevation $\mathcal{N}$. Trapezoidal cross sections, for example, lead to a fifth order polynomial under the square root (equation (76)), making it impossible to solve it using elliptic integrals. In the rest of this work we consider waves whose amplitude is not too large, so that $\mathcal{A}(\mathcal{N}), \tilde{d}(\mathcal{N})$ and $\widetilde{d^2}(\mathcal{N})$ can be with good accuracy Taylor-expanded as functions of $\mathcal{N}$. We first write

$$\mathcal{A}(\mathcal{N}) \approx 1 + \mathcal{N} + \tfrac{1}{2}\tau\mathcal{N}^2 + \tfrac{1}{3}\gamma\mathcal{N}^3 + \tfrac{1}{4}\varepsilon\mathcal{N}^4, \tag{87}$$

where τ, γ and ε are constants depending on the channel cross sectional shape. To be precise, denoting $M \doteq \cot\theta_l + \cot\theta_r$ where θ_l, θ_r are the left-bank and right-bank interior angles with the free surface in the rest state (see Figure 2), we define

$$\tau \doteq \frac{M\overline{d}}{B_0}, \tag{88}$$

which is twice the inverse of the dimensionless average bank slope, but will be referred to as the 'bank slope' in what follows. Similarly, γ is an average, dimensionless bank curvature in the rest state. We obtain

$$\tilde{d}(\mathcal{N}) \approx \overline{d}\left(1 - \tau\mathcal{N} + (\tau^2 - \tfrac{1}{2}\tau - \gamma)\mathcal{N}^2 - (\tau^3 - \tfrac{1}{2}\tau^2 - 2\gamma\tau + \tfrac{2}{3}\gamma + \varepsilon)\mathcal{N}^3\right), \tag{89}$$

$$\widetilde{d^2}(\mathcal{N}) \approx \overline{d^2}\left(1 - \tau\mathcal{N} + (\tau^2 - \gamma)\mathcal{N}^2 + (2\tau\gamma - \tau^3 - \varepsilon + \tfrac{1}{3}\tau\delta)\mathcal{N}^3\right), \tag{90}$$

with $\delta \doteq \overline{d}^2/\overline{d^2}$ as a shape factor of the cross section, and subsequently:

$$\frac{\overline{d^2}}{\overline{d}^2} - \mathcal{A}(\mathcal{N})\,\frac{\frac{\widetilde{d^2}(\mathcal{N})}{\overline{d}^2} - \mathcal{N}^2}{\frac{\tilde{d}(\mathcal{N})}{\overline{d}} + \mathcal{N}} \approx \mathcal{N}^2 + \tfrac{2}{3}\tau\mathcal{N}^3. \tag{91}$$

Equation (63) is thus approximated by

$$\frac{\xi}{d} \approx \pm \frac{1}{\sqrt{3\Lambda}} \int \frac{\mathrm{d}\mathcal{N}}{\sqrt{\mathcal{P}\left(\mathcal{N}\right)}}, \tag{92}$$

with the following definitions for the polynomial $\mathcal{P}\left(\mathcal{N}\right)$ and the constant Λ:

$$\mathcal{P}\left(\mathcal{N}\right) \doteq -\left(\mathcal{N}-\mathcal{N}_1\right)\left(\mathcal{N}-\mathcal{N}_2\right)\left(\mathcal{N}-\mathcal{N}_3\right) = P - Q\mathcal{N} + S\mathcal{N}^2 - \mathcal{N}^3; \tag{93}$$

$$\Lambda \doteq \tfrac{2}{3}\gamma C_0 - (\tau + \tfrac{2}{3}\gamma)C_1 + (1 + \tfrac{2}{3}\tau)\frac{C_2}{\mathcal{F}_0^2}, \tag{94}$$

and

$$\begin{aligned} P &\doteq \mathcal{N}_1\mathcal{N}_2\mathcal{N}_3 = \frac{1}{\Lambda}\left(1 - 2C_0 + C_1\right), \\ Q &\doteq \mathcal{N}_1\mathcal{N}_2 + \mathcal{N}_1\mathcal{N}_3 + \mathcal{N}_2\mathcal{N}_3 = \frac{2}{\Lambda}\left(C_0 - C_1\right), \\ S &\doteq \mathcal{N}_1 + \mathcal{N}_2 + \mathcal{N}_3 = \frac{1}{\Lambda}\left(-\tau C_0 + (1+\tau)C_1 - \frac{C_2}{\mathcal{F}_0^2}\right). \end{aligned} \tag{95}$$

The roots of $\mathcal{P}\left(\mathcal{N}\right)$ are ordered as follows: $\mathcal{N}_3 < \mathcal{N}_2 < \mathcal{N}_1$. With the classical variable change (see, *e.g.*, Korteweg and de Vries 1895, Violeau 2022) $\mathcal{N} = \mathcal{N}_2 + (\mathcal{N}_1 - \mathcal{N}_2)\cos^2\Psi$ we obtain a family of cnoidal waves, and Λ is rewritten as a function of P, Q, S, τ, γ:

$$\begin{aligned} \mathcal{N} &= \mathcal{N}_2 + (\mathcal{N}_1 - \mathcal{N}_2)\,\mathrm{cn}^2\left(\tfrac{1}{2}\sqrt{3\Lambda\left(\mathcal{N}_1 - \mathcal{N}_3\right)}\frac{x - ct}{d} \mid m\right), \\ m &\doteq \frac{\mathcal{N}_1 - \mathcal{N}_2}{\mathcal{N}_1 - \mathcal{N}_3}, \\ \Lambda &= \frac{1 - \frac{1}{3}\tau}{1 + \left(1 - \frac{1}{3}\tau\right)P + \left(1 + \frac{1}{6}\tau - \frac{1}{3}\gamma + \frac{1}{3}\tau^2\right)Q + \left(1 + \frac{2}{3}\tau\right)S}. \end{aligned} \tag{96}$$

where cn denotes Jacobi's elliptic cosine (Abramowitz and Stegun 1965). The wave length is

$$L = \frac{4K\left(m\right)}{\sqrt{3\Lambda\left(\mathcal{N}_1 - \mathcal{N}_3\right)}}, \tag{97}$$

with K the complete elliptic integral of the first kind (Abramowitz and Stegun 1965). As expected, we still have four degrees of freedom: $\mathcal{N}_1, \mathcal{N}_2, \mathcal{N}_3$ (or P, Q, S) and c. Note that the parameter ε defined in (87) has cancelled out, though it was necessary to obtain the above solution to the given order. Similarly, δ does not appear any more in the result, the only two parameters relative to the shape of the cross section being the dimensionless mean bank slope and curvature at rest, τ and γ. The rectangular section case ($\tau = \gamma = 0$) gives $\Lambda = \mathcal{F}_0^{-2}$ and $\mathcal{F}_0 = \sqrt{1 + P + Q + S} = \sqrt{(1 + \mathcal{N}_1)(1 + \mathcal{N}_2)(1 + \mathcal{N}_3)}$, in agreement with (El et al. 2006) (their equation (9)) as well as (Favrie and Gavriluk 2006).

Note that the approach proposed in the present section and the next one, *i.e.*, expanding the wave elevation up to a certain order, makes the present solution weakly non-linear, while the original equations where fully non-linear.

Soliton of moderate amplitude

We now investigate the case of solitary waves of moderate amplitude, *i.e.*, $(C_0, C_1, C_2) = (1, 1, 1)$, for which (94) shows that the channel bank curvature γ disappears from the model equations. Equations (64), (87) and (91) give the celerity of the solitary wave as a function of the bank slope τ and wave amplitude $\mathcal{N}^*$:

$$\frac{c_s}{\sqrt{g\bar{d}}} \approx 1 + \tfrac{1}{2}\left(1 - \tfrac{1}{3}\tau\right)\mathcal{N}^*, \tag{98}$$

in agreement with Fenton (1973) (his equation (4.6)). Note that Teng and Wu (1997)'s Boussinesq-type model, also investigated in Teng (2000), reads (after simplification and with our notations):

$$\frac{c_s}{\sqrt{g\bar{d}}} = \frac{1 + \mathcal{N}^*}{\mathcal{N}^*\left(1 + \tfrac{1}{2}\tau\mathcal{N}^*\right)}\sqrt{\frac{\tfrac{1}{2}\tau\mathcal{N}^{*2}(1 + \mathcal{N}^*) + (\tau - 2)\left(\mathcal{N}^* - (1 + \mathcal{N}^*)\ln(1 + \mathcal{N}^*)\right)}{1 + \tfrac{2}{3}\mathcal{N}^* - \tfrac{1}{3}\gamma\mathcal{N}^{*2}}}, \tag{99}$$

rendering (98), when expanded to the first order with respect to the wave amplitude. Additionally, Winckler and Liu (2015)'s formula (4.5b) leads to the same conclusion provided their coefficient γ (with a different meaning than the present one) is always negative, which is proved from its

definition (see Jouy et al. 2023).

The implicit solution (63) then gives

$$\frac{x - c_s t}{\overline{d}} \approx \pm \frac{\mathcal{F}_0}{\sqrt{3}} \int \frac{\mathrm{d}\mathcal{N}}{\mathcal{N}\sqrt{\mathcal{F}_0^2 - 1 - \left(1 + \frac{2}{3}\tau - \mathcal{F}_0^2 \tau\right)\mathcal{N}}}, \tag{100}$$

generalising the case of the rectangular section (66). From (100) it is easy to see that $\mathcal{F}_0^2 > 1$ is required, since the quantity under the square root must be positive. This is also in agreement with Fenton (1973). The solution to (100) is identical to the rectangular cross section case (67), with

$$\mathcal{N}^* = \frac{\mathcal{F}_0^2 - 1}{1 + \frac{2}{3}\tau - \mathcal{F}_0^2 \tau}, \tag{101}$$

rendering (68) in the rectangular cross section case. From (67) and (101), we also obtain the wavenumber k_s:

$$k_s \overline{d} = \tfrac{1}{2}\sqrt{\frac{(3 - \tau)\,\mathcal{N}^*}{1 + \left(1 + \frac{2}{3}\tau\right)\mathcal{N}^*}} \approx \tfrac{1}{2}\sqrt{(3 - \tau)\,\mathcal{N}^*}, \tag{102}$$

which, once more, agrees with Fenton's equation (4.7) (Fenton (1973)), but also with Peters (1968) and Peregrine (1968). Winckler and Liu (2015)'s equation (4.5a) contains more information on the channel cross section shape through their coefficient γ.

Equation (101) shows that the solitary wave amplitude can be negative if

$$\tau > \frac{3}{3\mathcal{F}_0^2 - 2} = \frac{3\,(1 + \tau\mathcal{N}^*)}{1 + 3\mathcal{N}^*}. \tag{103}$$

Substituting (101) into (103) and rearranging, we obtain the condition for the negative soliton as follows:

$$\tau > 3, \tag{104}$$

as stated by Peregrine (1968) from different considerations.

As an illustration, consider the case of a channel with trapezoidal section, *i.e.*, $M = 2m$ and

$\tau_{\text{trapezoid}} = 2\alpha$ from the definition (88) (recall α is defined by (74)–(75), giving $\tau_{\text{rectangle}} = 0$). Figure 4 shows the solution (67), (101) for various values of α and wave amplitude $\mathcal{N}^*$. One can see that the moderate amplitude solution is a good approximation of the true solution (76) obtained by numerical integration, as long as the dimensionless amplitude satisfies $\mathcal{N}^* \lesssim 0.1$. For the triangular cross-sectional case ($\alpha = \frac{1}{4}$), our equations (98) and (102) give the ratios of moderate amplitude solitary wave celerities and wavelengths λ_s, respectively:

$$\frac{c_{s,\text{triangle}}}{c_{s,\text{rectangle}}} \approx \frac{1 + \frac{5}{12}\mathcal{N}^*}{1 + \frac{1}{2}\mathcal{N}^*} \approx 1 - \tfrac{1}{12}\mathcal{N}^*, \tag{105}$$

$$\frac{\lambda_{s,\text{triangle}}}{\lambda_{s,\text{rectangle}}} \approx \sqrt{\frac{3 - \tau_{\text{rectangle}}}{3 - \tau_{\text{triangle}}}} = \sqrt{\tfrac{6}{5}} \approx 1.0954. \tag{106}$$

Teng (2000) shows that Teng and Wu (1997)'s model agrees that the wavelength on a triangular-section channel should be larger than that in a rectangular section, but no analytical formula is given. Teng's Figure 3 is qualitatively in agreement with the present Figure 6, showing the free surface elevation at a given time in both channels with the present model, when the dimensionless amplitude $\mathcal{N}^* = 0.3$. The same kind of behavior is reported by Winckler and Liu (2015)'s Figure 4. On the other hand, Teng and Wu (1997) found a higher wavelength than the present model for the triangular case, typically 1.3 times the wavelength in the rectangular channel for $\mathcal{N}^* = 0.3$. They findings are supported by laboratory measurements, but their experimental soliton is of poor quality and should not be considered as a reference. High quality experimental solitary waves in channels of non-rectangular cross sections are still missing in the current literature.

Teng (2000) also investigates a triangular section with vertical walls above the rest free surface, showing a different behaviour than with the rectangular and triangular sections. Our model does not provide such a prediction, since for any cross section with vertical walls we have $A = A_0 + B_0\tilde{\eta}$, hence $\mathcal{A}(\mathcal{N}) = 1 + \mathcal{N}$; moreover, both integrals in (14) and (15) are calculated with the same

bounds, therefore $\tilde{d}\left(\mathcal{N}\right) = \overline{d}$ and $\widetilde{d^2}\left(\mathcal{N}\right) = \overline{d^2}$, and the general travelling wave solution reduces to

$$\frac{x - ct}{\overline{d}} = \pm \int \frac{\mathrm{d}\mathcal{N}}{\sqrt{3\left[1 - 2C_0\left(1 + \mathcal{N}\right) + C_1\left(1 + \mathcal{N}\right)^2 + \frac{C_2}{\mathcal{F}_0^2}\left(1 + \mathcal{N}\right)\mathcal{N}^2\right]}}, \tag{107}$$

as for a rectangular section. To circumvent this issue, it would be necessary to build more advanced governing equations accounting for the bottom kinematic boundary condition in the Lagrangian (37), which requires a non-zero transverse velocity, thus a free surface that varies along the channel width as in Teng and Wu (1997) and Winckler and Liu (2015).

Application: undular bore's leading wave

The leading wave of an Undular bore is known to behave like a solitary wave (El et al. 2006, Violeau 2022). In a trapezoidal channel, equation (79) should thus be valid for linking the leading wave amplitude $\mathcal{N}^*$ and the upstream Froude number $\mathcal{F}_0$. Sandover and Taylor (1962) performed undular bores experiments in a channel of trapezoidal cross-section with variable slope angle, and discuss the variability of the leading wave amplitude; they conclude that this is an effect of the cross-sectional shape, thus of the slope angle θ defined in Figure 3. They made their data dimensionless using the rest water depth h_0 (while the present study proves that the mean water depth at rest $\overline{d} = \frac{1+\beta}{1+2\beta}h_0$ is more relevant). With this correction, Figure 7 shows that equation (79) agrees with Sandover and Taylor (1962)'s experiments for various slope angles and channel flowrates, confirming that the present model is relevant to describe the influence of the cross-section shape on the dynamics of dispersive waves.

Conclusions

The variety of circumstances were dispersive, non linear waves occur in channels makes it necessary to propose alternatives to the classical channel, section-averaged, Saint-Venant equations, which fail in predicting all situations where the vertical component of the velocity field makes the pressure non-hydrostatic. While Boussinesq-type models remain weakly non-linear, the present approach is fully non-linear, though restricted to weakly dispersive waves and wave trains.

The variational method proposed by Clamond and Dutykh (2012) proved to be efficient in finding a system of Serre equations for arbitrary cross-sectional channels, given by (24), (40) and (45), the derivation being significantly easier than it would be by using the more traditional asymptotic expansion approach as in Debyaoui and Ersoy (2020). The global family of travelling waves (63) including solitary waves with celerity (64) are formally written for arbitrary shape of the cross section through the bottom/bank elevation $d(y)$. Hager and Hutter (1984)'s method allows writing an upper bound of the wave elevation as a function of the Froude number, and the present theory agrees, up to the first order, with Hager and Hutter (1984)'s model for trapezoidal cross sections. For waves of moderate amplitude, a simplification of the proposed model, closer to the Boussinesq approach, is able to predict the main wave characteristics as functions of the channel dimensionless bank slope τ, and curvature γ. The solitary wave of moderate amplitude is of particular interest, the proposed model giving the celerity and wave number as functions of τ in agreement with well-established results of the existing literature. Peregrine's negative-soliton criterion for τ is also recovered to the leading order.

The data available in the literature regarding travelling waves in non-rectangular cross-sectional channels being scarce and of modest quality, it was not possible to propose a quantitative application of the present model in documented realistic cases. On the contrary, waves with non-uniform celerity like undular bores have been extensively studied in flumes (*i.e.*, Favre 1935 and Treske 1994), but their complete theoretical analysis would require a particular treatment based on a modulation theory, which was not possible within the extent of the present work. Modeling these bores, as well as more complex situations in practical engineering applications, would benefit from a space-time numerical integration of the proposed governing equations. Numerical scheme based on the classical Serre–Green–Naghdi have already been successfully used in this context (Chassagne et al. 2019, Biswas et al. 2021), giving interesting clues for the numerical treatment of the proposed equations.

It is noteworthy that the model proposed herein was based on some strong assumptions. One of the most important is the uniformity of the free surface elevation along the channel (or river)

width. This makes it impossible to predict situations were the free surface experiences a transverse curvature, as it has been observed in non-rectangular cross-sectional channels (Peregrine 1968, Treske 1994). In such cases, the wave celerity is non-uniform along the width and waves easily break near the banks, leading to various specific phenomena (Chassagne et al. 2019, Violeau 2022). The present model thus paves the way for more sophisticated theoretical developments, including a more advanced model accounting for the bed kinematics boundary condition, as well as transverse velocity and free surface variation. Such an approach would allow treating the variabiliy of the free surface across the channel width. Whitham's modulation theory, recently investigated in the framework of the Serre–Green–Naghdi equations (El et al. 2006, Tkachenko et al. 2020), may also be used to extend the present model to the prediction of channel dispersive shock waves, including the complete above-mentioned Favre waves, as well as tidal bores.

From the analysis of the results of the present model, it can be concluded that non-hydrostatic models, either weakly non-linear like Boussinesq models, or fully non-linear like Serre models, are not a luxury but a necessity. As demonstrated by the application example depicted in the last section, with the present model the amplitude of the leading soliton of Favre waves in hydropower channels can be predicted as a function of the bank slope with a fairly good accuracy. Such a prediction could not be achieved with the non-linear shallow water (Saint-Venant) equations, which predict a hydraulic jump for all upstream Froude numbers. The leading wave of Favre dispersive wave trains having an amplitude close to twice the corresponding hydraulic jump, the improvement due to non-hydrostatic models is of prime importance for flooding safety and waterworks design.

NOTATION

The following symbols are used in this paper:

$[\varphi]$ = vertical average of φ;

$\widetilde{\varphi}$ = width-average of φ;

$\overline{\varphi}$ = width-average of φ in rest state;

$\langle\varphi\rangle$ = section-average of φ;

$\hat{\varphi}$ = free surface value of φ;

$\check{\varphi}$ = bottom value of φ;

A = channel cross section (m^2);

A_0 = channel cross section at rest (m^2);

$\mathcal{A}$ = dimensionless channel cross section (–);

B = channel width (m);

B_0 = channel width at rest (m);

B^l = channel left bank distance (m);

B^r = channel right bank distance (m);

B_0^l = channel left bank distance at rest (–);

B_0^r = channel right bank distance at rest (–);

c, c_s = wave celerities (m/s);

d = bottom depth (m);

$\mathcal{F}_0$ = Froude number (–);

g = gravity acceleration (m^2/s);

h = water depth (m);

k_s = soliton wave number (s^{-1});

$\mathscr{L}$ = Lagrangian (m^5/s);

$\mathcal{L}$ = Lagrangian density (m^3/s^2);

$\mathcal{N}$ = dimensionless free surface elevation (–);

$\mathcal{N}^*$ = dimensionless wave amplitude (–);

t = time (s);

$\mathbf{u} = (u, v)$ = horizontal velocity field (m/s);

w = vertical velocity field (m/s);

$\mathbf{x} = (x, y)$ = horizontal coordinates (m);

z = vertical coordinate (m);

α, β = shape factors of trapezoidal channel (–);

γ = dimensionless bank curvature (–);

η = free surface elevation (m);

Θ = mean bottom angle (rad);

θ = slope angle of a trapezoidal channel (rad);

$\lambda = (\lambda, \mu)$ = horizontal conjugate velocity field (m/s);

λ_s = soliton wave length (m);

ν = vertical conjugate velocity field (m/s);

τ = dimensionless bank slope (–); and

ϕ = velocity potential (m^2/s).

DATA AVAILABILITY STATEMENT

No data, models, or code were generated or used during the study.

ACKNOWLEDGMENTS

This work was funded by EDF. The author is grateful to Prof. Oscar Castro-Orgaz (Universidad de Córdoba, Spain) for inviting him to contribute to this special issue. He also wants to thanks Prof. Willi Hager (ETH Zurich, Switzerland) his fruitful comments that helped him on improving his work. He is also indebted to an anonymous reviewer for providing useful comments and advice on the original manuscript. All formulae and figures were checked with Scientific WorkPlace 5.5.

SUPPLEMENTARY MATERIALS

Equations (S1) to (S9) are available online in the ASCE Library (ascelibrary.org).

REFERENCES

Abramowitz, M. and Stegun, I. (1965). *Handbook of Mathematical Functions: With Formulas, Graphs, and Mathematical Tables*. Dover Publications, New York.

549 Biswas, T., Dey, S., and Sen, D. (2021). "Modeling positive surge propagation in open channels
550 using the Serre–Green–Naghdi equations." *Appl. Math. Model.*, 97, 803—-820.
551 Carter, J. and Cienfuegos, R. (2011). "The kinematics and stability of solitary and cnoidal wave
552 solutions of the serre equations." *Eur. J. Mech. B/Fluids*, 30, 259–268.
553 Castro-Orgaz, O., Hager, W., and Cantero-Chinchilla, F. (2022). "Shallow flows over curved beds:
554 Application of the Serre-Green-Naghdi theory to weir flow." *J. Hydr. Engng.*, 148(1).
555 Chanson, H. (2011). *Tidal Bores, Aegir, Eagre, Mascaret, Pororoca: Theory and Observations*.
556 World Scientific, Singapore.
557 Chassagne, R., Filippini, A., Ricchiuto, M., and Bonneton, P. (2019). "Dispersive and dispersive-
558 like bores in channels with sloping banks." *J. Fluid Mech.*, 870, 595—-616.
559 Clamond, D. and Dutykh, D. (2012). "Practical use of variational principles for modeling water
560 waves." *Phys. D*, 241(1), 25–36.
561 Clamond, D., Dutykh, D., and Mitsotakis, D. (2017). "Conservative modified Serre-Green-Naghdi
562 equations with improved dispersion characteristics." *Comm. Nonlin. Sci. Numer. Simul.*, 45,
563 245–257.
564 Daily, J. and Stephans, C. (1952). "The solitary wave." *Proc. Third Conf. Coastal Engineering*,
565 13—-30.
566 Debyaoui, M. and Ersoy, M. (2020). "Generalised Serre–Green–Naghdi equations for open channel
567 and for natural river hydraulics." *Asympt. Anal.*, 124(3-4), 343–369.
568 El, G., Grimshaw, R., and Smyth, N. (2006). "Unsteady undular bores in fully nonlinear shallow-
569 water theory." *Phys. Fluids*, 18, 27104.
570 Favre, H. (1935). *Etude théorique et expérimentale des ondes de translation dans les canaux*
571 *découverts*. Dunod, Paris, France (in French).
572 Favrie, N. and Gavriluk, S. (2006). "A rapid numerical method for solving Serre–Green–Naghdi
573 equations describing long free surface gravity waves." *Nonlinearity*, 30(7), 2718.
574 Fenton, J. (1973). "Cnoidal waves and bores in uniform channels of arbitrary cross-section." *J.*
575 *Fluid Mech.*, 58(3), 417–434.

Green, A., Laws, N., and Naghdi, P. (1974). "On the theory of water waves." *Proc. R. Soc. Lond. A*, 338, 43—-55.

Green, A. and Naghdi, P. (1976). "A derivation of equations for wave propagation in water of variable depth." *J. Fluid Mech.*, 78(2), 237–246.

Hager, W. and Hutter, K. (1984). "Approximate treatment of plane channel flow." *Acta Mech.*, 51, 31—-48.

Jouy, B., Le, M., Ricchiuto, M., and Violeau, D. (2023). "A numerical model of channel Favre waves." *in preparation*.

Korteweg, D. and de Vries, G. (1895). "On the change of form of long waves advancing in a rectangular canal, and on a new type of long stationary waves." *Phil. Mag.*, 39(240), 422—-443.

Luke, J. (1967). "A variational principle for a fluid with a free surface." *J. Fluid Mech.*, 27(2), 375–397.

Mohapatra, P. and Chaudhry, M. (2004). "Numerical solution of Boussinesq equations to simulate dam-break flows." *J. Hydraulic Engng.*, 130(2), 156—-159.

Mohapatra, P., Eswaran, V., and Murthy Bhallamudi, S. (1999). "Two-dimensional analysis of dam-break flow in a vertical plane." *J. Hydraulic Engng.*, 125(2), 183—-192.

Peregrine, D. (1968). "Long waves in a uniform channel of arbitrary cross-section." *J. Fluid Mech.*, 32(2), 353–365.

Peregrine, D. (1969). "Solitary waves in trapezoidal channels." *J. Fluid Mech.*, 35(1), 1—-6.

Peters, A. (1968). "Rotational and irrotational solitary waves in a channel with arbitrary cross section." *Comm. Pure Appl. Math.*, 19(4), 445–471.

Sandover, J. and Taylor, C. (1962). "Cnoidal waves and bores." *La Houille Blanche*, 3, 443—-455.

Seabra-Santos, F., Renouard, D., and Temperville, A. (1987). "Numerical and experimental study of the transformation of a solitary wave over a shelf or isolated obstacle." *J. Fluid Mech.*, 176, 117—-134.

Serre, F. (1953a). "Contribution à l'étude des écoulements permanents et variables dans les canaux." *La Houille Blanche*, 39(3), 374–388 in French.

603 Serre, F. (1953b). "Contribution à l'étude des écoulements permanents et variables dans les canaux."
604 *La Houille Blanche*, 39(6), 830–872 in French.
605 Su, C. and Gardner, C. (1969). "KdV equation and generalizations. Part iii. Derivation of the
606 Korteweg-de Vries equation and Burgers equation." *J. Math. Phys.*, 10(3), 536—-539.
607 Teng, M. (2000). "Boussinesq solution for solitary waves in uniform channels with sloping walls."
608 *J. Mech. Eng. Sc.*, 214(6), 781–787.
609 Teng, M. and Wu, T. (1997). "Effects of channel cross-sectional geometry on long wave generation
610 and propagation." *Phys. Fluids*, 9(11), 3368–3377.
611 Tkachenko, S., Gavriluk, S., and Shuye, K.-M. (2020). "Hyperbolicity of the modulation equations
612 for the Serre-Green-Naghdi model." *Water waves*, 2, 299–326.
613 Treske, A. (1994). "Undular bores (Favre waves) in open channels. Experimental studies." *J. Hydr.*
614 *Res.*, 32(3), 355—-370.
615 Violeau, D. (2022). "Contribution to the theory of undular bores. a journey around the Korteweg—
616 de Vries equation." *IAHR Water Monographs Series*, <https://www.iahr.org/index/detail/659>.
617 Winckler, P. and Liu, P.-F. (2015). "Long waves in a straight channel with non-uniform cross-
618 section." *J. Fluid Mech.*, 770, 156–188.

List of Figures

Fig. 1. View of the channel of the Sisteron dam (EDF, France). Favre waves are propagating upstream after gate closure. Photo EDF/CIH.

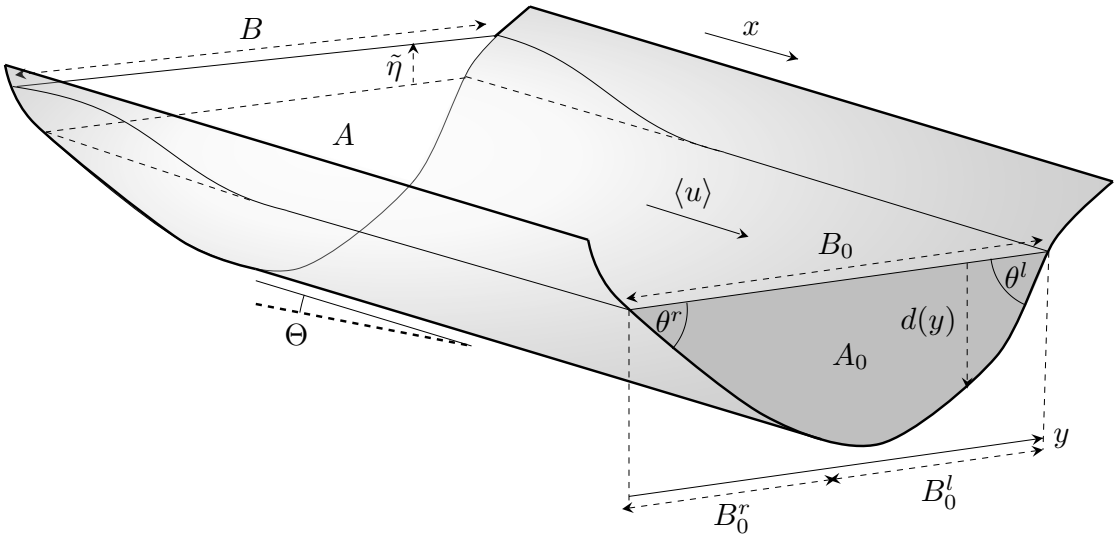

Fig. 2. Notation: prismatic channel with uniform free surface across the width.

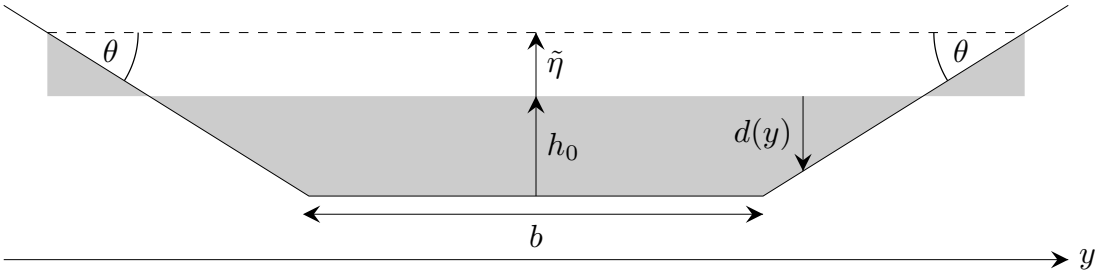

Fig. 3. Notation: the trapezoidal cross sectional case. The rest water depth $d(y)$ is considered positive when the bed elevation is below the rest free surface; it it thus negative in the side gray triangles.

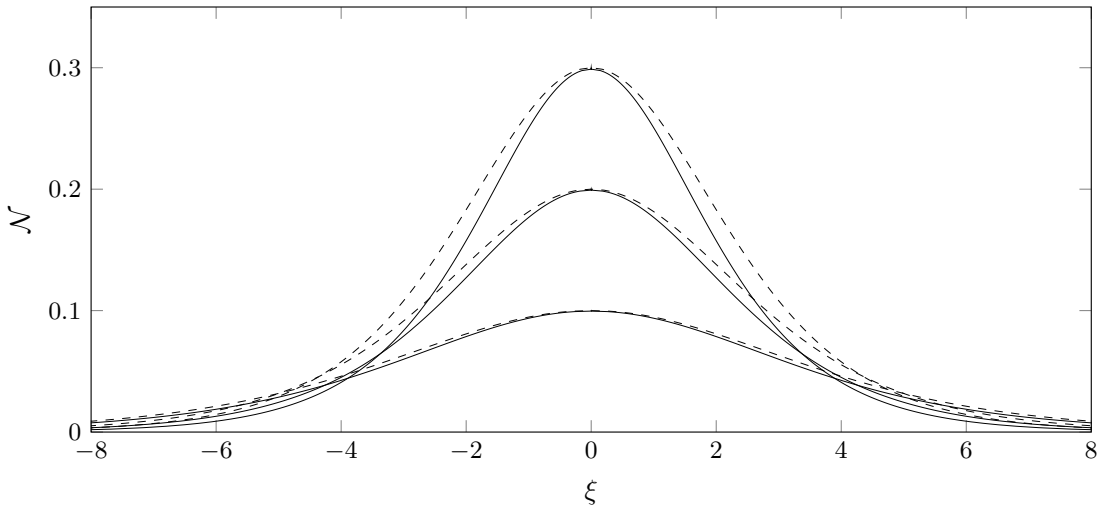

Fig. 4. Solitary wave with $\alpha = 0.25$ (triangular cross section) and wave amplitude $\mathcal{N}^* = 0.1, 0.2, 0.3$. (—) numerical integration of of (76); (- - -) equations (67) and (101).

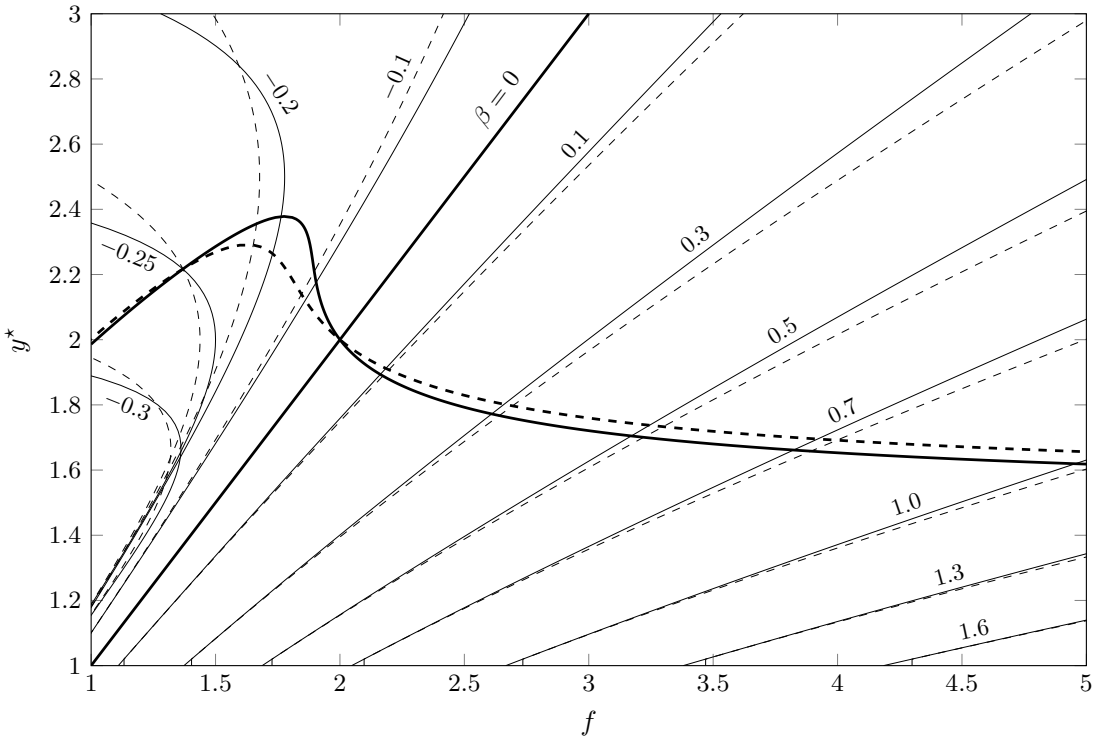

Fig. 5. Variation of the wave elevation y^* with the Froude number squared f in a trapezoidal channel for various values of β; (—) present model (80); (- - -) Hager and Hutter's model (see Supplementary Materials, (S6)). The thick lines show the critical wave amplitude $y_c^*(f)$ given by (86) and (S8)–(S9), with the same convention.

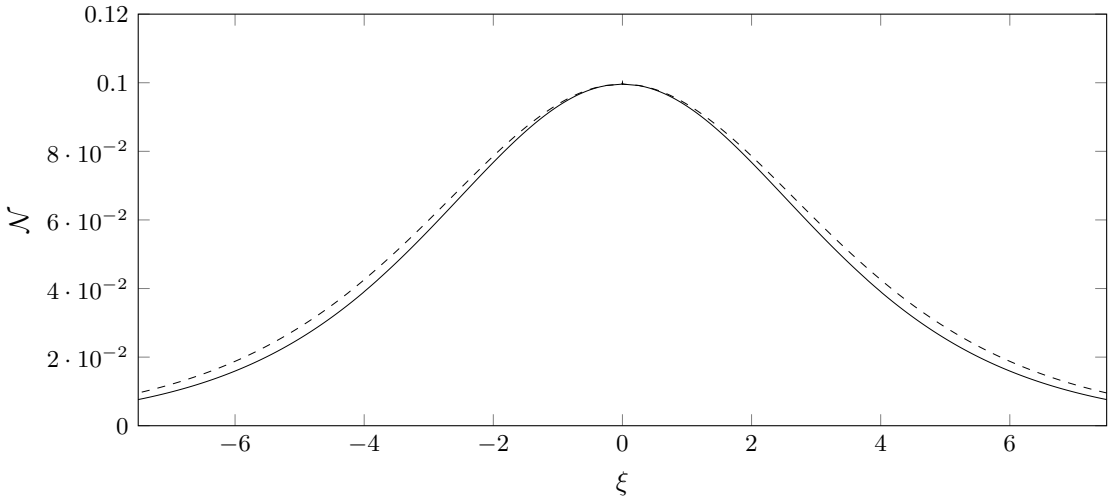

Fig. 6. Numerical integration of the solitary wave solution (76) with amplitude $\mathcal{N}^* = 0.3$; (—-) rectangular channel section ($\tau = 0$); (- - -) triangular section ($\tau = \frac{1}{2}$).

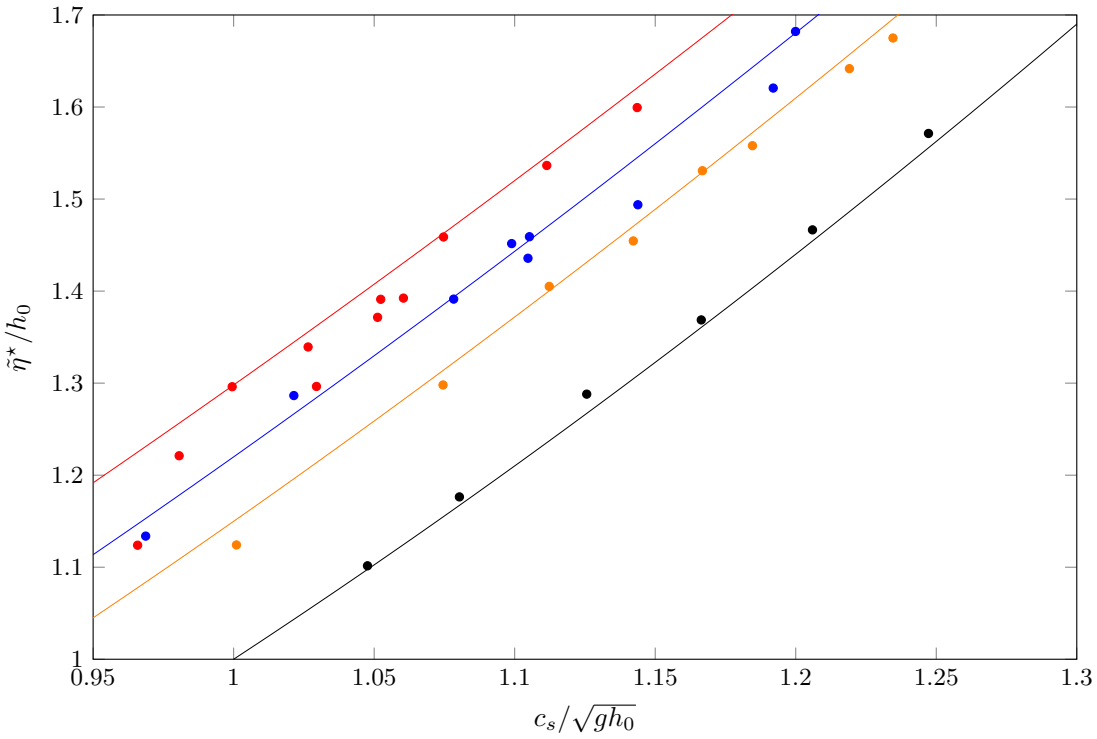

Fig. 7. Amplitude of the leading soliton of an undular bore as a function of the Froude number. Both quantities are based on the initial water depth h_0 to allow comparison with data. Solid lines: equation (79); symbols: experiments. The channel section is trapezoidal as in Figure 3, with different values of the slope angle: $\theta = 90°$ (black, rectangular section), 60° (orange), 45° (blue) and 30° (red).